Enhanced spin coherence of rubidium atoms in solid parahydrogen

Sunil Upadhyay,[1] Ugne Dargyte,[1] Robert P. Prater,[1] Vsevolod D. Dergachev,[2] Sergey A. Varganov,[2] Timur V. Tscherbul,[1] David Patterson,[3] and Jonathan D. Weinstein[1,*]

[1]*Department of Physics, University of Nevada, Reno, Nevada 89557, USA*

[2]*Department of Chemistry, University of Nevada, Reno, Nevada 89557, USA*

[3]*Broida Hall, University of California, Santa Barbara, Santa Barbara, California 93106, USA*

(Received 28 November 2018; published 15 July 2019)

We measure the transverse relaxation of the spin state of an ensemble of ground-state rubidium atoms trapped in solid parahydrogen at cryogenic temperatures. We find the spin dephasing time of the ensemble (T_2^*) is limited by inhomogeneous broadening. We determine that this broadening is dominated by electrostaticlike interactions with the host matrix, and can be reduced by preparing nonclassical spin superposition states. Driving these superposition states gives significantly narrower electron paramagnetic resonance lines and the longest reported electron spin T_2^* in any solid-phase system other than solid helium.

DOI: 10.1103/PhysRevB.100.024106

Measuring the energy splitting between Zeeman levels is at the heart of atomic magnetometry [1], electron paramagnetic resonance (EPR) spectroscopy [2], and fundamental physics measurements [3–5]. For an ensemble of N atoms, the shot-noise limited precision of a single measurement is $\sigma_E \sim \frac{\hbar}{T_2^*\sqrt{N}}$ [1], where T_2^* is the ensemble's spin dephasing time. In this paper, we show that rubidium atoms in parahydrogen have favorable T_2^* times for a solid state electron spin ensemble. Moreover, their T_2^* can be further extended by using nonclassical superposition states instead of traditional Larmor precession states.

Our apparatus is similar to that described in Refs. [6,7]. We grow our crystal by codepositing hydrogen and rubidium gases onto a cryogenically cooled sapphire window at 3 K. We enrich the parahydrogen fraction of hydrogen by flowing the gas over a cryogenically cooled catalyst. In the data presented in this paper, the orthohydrogen fraction is $<10^{-4}$. Typical thicknesses of the doped crystals are $\sim$0.3 mm. We use natural-isotopic-abundance rubidium; typical rubidium densities are on the order of 10^{17} cm^{-3}, or a few ppm.

We apply a static "bias" magnetic field (B_z) normal to the surface of the crystal. We polarize the spin state of the implanted Rb atoms by optically pumping the atoms with a circularly polarized laser. To minimize magnetic field inhomogeneities across the sample we optically select a region of the crystal with transverse dimensions of roughly $\sim$0.1 mm. We measure the polarization through circular dichroism, measuring the relative transmission of left-handed and right-handed circularly polarized light (LHC and RHC). As described in Ref. [6], the circular dichroism signals observed are roughly an order of magnitude smaller than for gas-phase atoms, and we are unable to determine if the reduced signal is due to imperfect optical pumping, readout, or both. Hence our "effective" atom number in a typical measurement is $\sim$10% of the $\sim 10^{12}$ atoms in a typical sample volume. Larger number samples could be obtained by using larger-diameter beams (or a thicker crystal) to address a larger volume of atoms.

We drive transitions between Zeeman states with transverse rf magnetic fields generated by a wire a few mm above the surface of the crystal. We take data with bias fields ranging from 40 to 120 G, giving Zeeman shifts that are small compared to the hyperfine splitting, but sufficiently large that transitions between different Zeeman levels can be spectrally resolved. The level structure of ground-state ^{85}Rb is shown in Fig. 1. In the gas phase, the hyperfine splitting is 3.0357 GHz [8]. From prior work, the hyperfine constants of alkali-metal atoms in noble gas matrices are within a few percent of the free-space atom value [9]; we expect alkali-metal atoms in parahydrogen to be similar.

We measure rubidium's transverse relaxation time by free-induction-decay (FID) measurements. After polarizing the spin through optical pumping, an rf pulse is applied to induce Larmor precession. The Larmor precession and its decay are measured optically via circular dichroism [1]. The measured values of T_2^* are on the order of 10 μs or shorter, as presented in the Supplemental Material [10].

This is significantly shorter than spin-echo measurements under similar conditions (which indicate $T_2 \gtrsim 1$ ms). This indicates that the dominant limit on T_2^* comes from static inhomogeneous broadening (static on the spin-echo timescale). Significant inhomogeneous broadening is not surprising, given that our matrix growth conditions are expected to produce polycrystalline parahydrogen [11,12].

For a magnetically pure host such as parahydrogen, we hypothesize that the observed inhomogeneous broadening is dominated by electrostatic interactions. We note that the Hamiltonian for electrostatic interactions is unchanged under time reversal. Thus, to first order in the perturbation, the electrostatic energy shift of a state $|\psi\rangle$ and its time-reversed state $|\tilde{\psi}\rangle$ must be identical. A superposition state of Zeeman levels which are time reversals of each other will have a reduced inhomogeneous broadening. For free-space Rb atoms, $|F, \pm m_F\rangle$ pairs are time reversals of each other in the low-field limit (the stretched states $|F = I + J, m_F = \pm F\rangle$ are time reversals of

*weinstein@physics.unr.edu; http://www.weinsteinlab.org

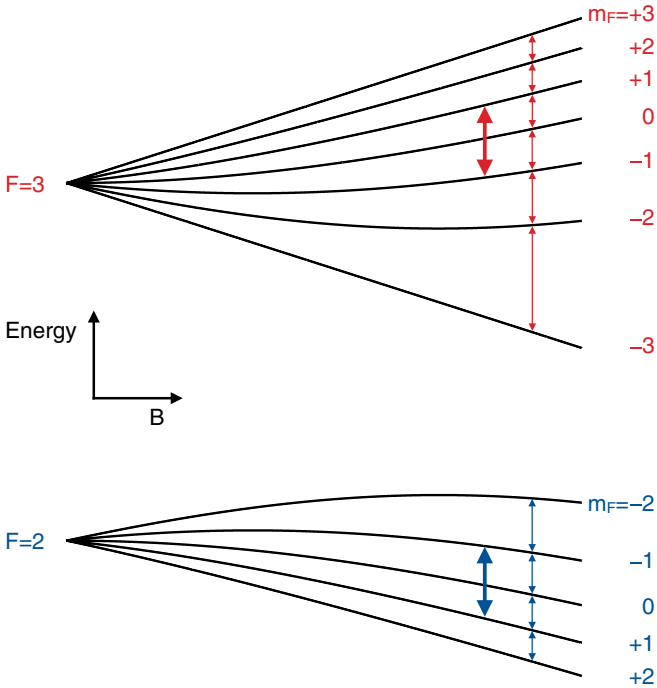

FIG. 1. Schematic of the Zeeman levels of gas-phase ^{85}Rb, showing some of the relevant transitions of Fig. 2. The energy eigenstates (black) are labeled by their low-field quantum numbers F and m_F, and we refer to them throughout the paper by that terminology. The slender arrows denote the single-photon transitions. The wide arrows denote the two-photon transitions between states which are approximate time reversals of each other; each two-photon transition is shown as a single arrow. To better illustrate the nondegenerate frequencies of the transitions, the Zeeman levels are plotted over a larger range of magnetic fields than used in this experiment; likewise, the transition arrows are horizontally offset for ease of viewing.

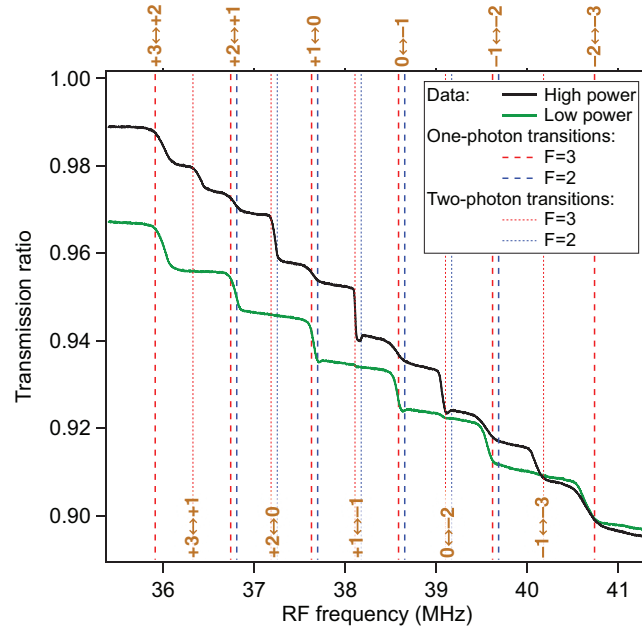

FIG. 2. Depolarization spectroscopy signals, as discussed in the text, taken with $B_z = 82$ G. The vertical axis measures the ratio of the transmission of LHC and RHC probe beams; under conditions of no spin polarization the ratio is 1. The signal is plotted as a function of the rf frequency; in these data the rf is swept from high to low frequency. The dashed vertical lines mark the calculated single-photon and two-photon transition frequencies for gas-phase ^{85}Rb [13]; the yellow labels denote $m_F \leftrightarrow m_F'$.

each other at all fields). We can use multiphoton transitions, as shown in Fig. 1, to prepare superpositions of this kind.

Superpositions of these states cannot be studied by FID techniques. Only superpositions of Zeeman levels which differ by $\Delta m = 1$ give rise to Larmor precession. For the superpositions of interest, the expectation value of the spin projection along a transverse axis is zero. Thus there is no *literal* "transverse spin relaxation" time. However, as any other two-level system, a superposition of $|m_F = +1\rangle$ and $|m_F = -1\rangle$ has a well-defined dephasing time.

To measure T_2^* we use "depolarization spectroscopy," wherein we polarize the atoms by optical pumping, then continuously measure the circular dichroism signal as we scan the rf frequency across the resonances. When the frequency is on resonance between two m_F energy eigenstates, population is transferred between them and the polarization signal changes. In the limit of low rf power and a slow frequency sweep, the linewidth of the transition provides a measurement of the inhomogeneous broadening and hence T_2^*.

Figure 2 shows depolarization data for ^{85}Rb at two different rf powers. For the low-power sweep, we see a change in the polarization signal at each expected single-photon resonance frequency. The broadening is sufficiently large that the $F = 2$ transitions are not fully resolved from the $F = 3$ transitions. At higher powers, the two-photon transitions become observable. The $+1 \leftrightarrow -1$ transitions at the center of the spectrum are significantly narrower than all other one- and two-photon transitions. This is precisely as expected for inhomogeneous electrostatic broadening, as they are the only two-photon transitions between time-reversed states. This confirms that the dominant inhomogeneous broadening mechanism is time-even in nature (electrostaticlike), as time-odd (magnetostaticlike) perturbations would result in a $+1 \leftrightarrow -1$ linewidth approximately twice that of a $0 \leftrightarrow \pm 1$ transition.

For the $+1 \leftrightarrow -1$ transitions, the $F = 2$ and $F = 3$ transitions are cleanly resolved; the two transitions cause the circular dichroism signal to change in opposite directions.

We extract linewidths from these data by assuming the inhomogeneous broadening is Gaussian and fitting each transition in the depolarization spectrum to a corresponding error function. The extracted linewidths as a function of magnetic field are shown in Fig. 3 for ^{85}Rb and ^{87}Rb. These linewidths reflect low-field (i.e., non-power-broadened) values. For the single-photon transitions, the linewidths measured through depolarization spectroscopy match those from FID measurements to within our experimental error. A comparison is provided in the Supplemental Material [10].

Examining the single-photon linewidths in Fig. 3, we see that ^{87}Rb exhibits more broadening than ^{85}Rb. This is as one would naively expect for shifts that are electrostatic in nature, as tensor Stark shifts are larger for ground-state ^{87}Rb ($F = 2$) than for ^{85}Rb ($F = 3$) [14]. For a static electric field, calculations predict the $\pm 1 \leftrightarrow 0$ transitions in ^{87}Rb ($F = 2$) would

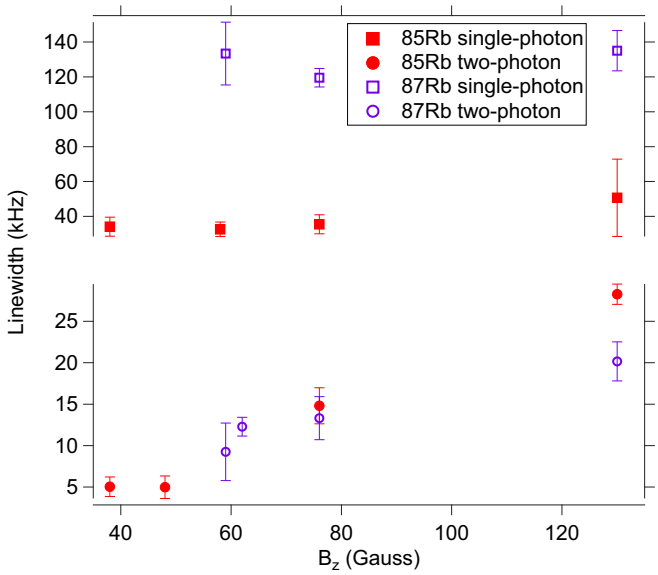

FIG. 3. Measured linewidths of ^{85}Rb in the $F = 3$ hyperfine state and ^{87}Rb in the $F = 2$ hyperfine state. For the single-photon linewidth, we plot the average of the $|m_F = \pm 1\rangle \leftrightarrow |m_F = 0\rangle$ transitions. For the two-photon linewidth we plot the linewidth of the $+1 \leftrightarrow -1$ transition.

show 3.2 times the tensor Stark shift of ^{85}Rb ($F = 3$) [14], consistent with the differences seen in the linewidths of Fig. 3.

We attribute the dominant contribution to the linewidth of the $+1 \leftrightarrow -1$ transitions to residual electrostatic broadening that arises because these energy eigenstates are not perfect time reversals of each other. While we do not know the exact form of the tensor interaction with the parahydrogen host, we can use perturbation theory to qualitatively predict the linewidth of the $+1 \leftrightarrow -1$ transition. We consider an atom with hyperfine constant of A, a Zeeman splitting of z, and an interaction with the matrix which is symmetric under time reversal and on the order of m. We consider the limit that $A \gg z \gg m$, and only include perturbations from m to lowest-order in perturbation theory. In this limit, we expect the linewidth of the $+1 \leftrightarrow -1$ transition to be smaller than the single-photon transitions by a factor of $\sim \frac{z}{A}$ (ignoring numerical prefactors). The residual broadening is due to the breakdown of the time-reversal symmetry of the $|+1\rangle$ and $|-1\rangle$ energy eigenstates at nonzero magnetic field. This model qualitatively agrees with our linewidth measurements (Fig. 3), and explains the observed dependence of the $+1 \leftrightarrow -1$ linewidth on the magnetic field. We note that measurements of ^{85}Rb as a function of rubidium density indicate that dipolar broadening does not contribute significantly to the linewidth.

The only energy eigenstates of the free atom which are time reversals of each other at all magnetic fields are the "stretched states": $|F = 3, m_F = \pm 3\rangle$ for ^{85}Rb and $|F = 2, m_F = \pm 2\rangle$ for ^{87}Rb. Inhomogeneous electrostatic broadening should be further suppressed for these states. We have not been successful in observing the six-photon $+3 \leftrightarrow -3$ transition in ^{85}Rb; we suspect this is due to insufficient rf power. Observations of the four-photon $+2 \leftrightarrow -2$ transition in ^{87}Rb at 60 G indicated narrower lines, but not at a statistically significant level. We suspect the measured linewidth of the ^{87}Rb stretched state transition is limited by technical limitations of our apparatus (magnetic field gradients, as well as magnetic field instabilities which prevent averaging) and possible coupling to other states in the multiphoton transition.

To estimate the matrix shifts of the alkali-metal atoms trapped in solid p-H_2, we use a third-order perturbative expression [15]

$$\Delta E_{\rm hf} = \sum_{ij}\sum_{kl} \frac{\langle 00|V_{dd}|ij\rangle\langle ij|H_{\rm hf}|kl\rangle\langle kl|V_{dd}|00\rangle}{(E_{00}-E_{ij})(E_{00}-E_{kl})} - \langle 00|H_{\rm hf}|00\rangle \sum_{kl} \frac{\langle 00|V_{dd}|kl\rangle\langle kl|V_{dd}|00\rangle}{(E_{00}-E_{kl})^2}, \quad (1)$$

where the unperturbed basis functions $|ij\rangle = |i\rangle_A|j\rangle_{\rm H_2}$ describe the electronic states of noninteracting atom A and H_2, with energies $E_{kl} = E_k^A + E_l^{\rm H_2}$ and $H_{\rm hf}$ is the atomic hyperfine Hamiltonian [8], and V_{dd} is the dipole-dipole interaction [15]. The sums in Eq. (1) run over all excited electronic, fine, and hyperfine states of A and H_2. The first term in Eq. (1) gives rise to an m_F-dependent tensor matrix shift of the atomic hyperfine levels [16] whereas the second term leads to an m_F-independent scalar shift $\Delta E^s_{\rm hf}$. The latter can be estimated by assuming that $E_{00} - E_{ik} \simeq E_A + E_{\rm H_2}$, where E_A is the average excitation energy of atom A and $E_{\rm H_2}$ is that of H_2 [15]. Using the closure relation to eliminate the summations over the excited states in the second term of Eq. (1), we obtain [15]

$$\Delta E^s_{\rm hf} \simeq -\langle 00|H_{\rm hf}|00\rangle \left(\frac{1}{E_A + E_{\rm H_2}}\right) E_{\rm disp}, \quad (2)$$

where $E_{\rm disp} = \langle 00|V_{dd}^2|00\rangle/(E_A + E_{\rm H_2})$ is the dispersion interaction energy of A with H_2.

To estimate the tensor matrix shift, we take into account only the diagonal matrix elements of the hyperfine interaction in Eq. (1) and assume that $\langle i|H_{\rm hf}|i\rangle \simeq A_P$ is independent of the electronic state i and equal to the hyperfine constant of the lowest excited $^2P_{1/2}$ state of atom A. Since the hyperfine constants of alkali-metal atoms decrease rapidly with increasing i [8], these assumptions provide a conservative upper bound to the magnitude of the tensor shift

$$\Delta E^t_{\rm hf} < A_P \sum_{i,j} \frac{\langle 00|V_{dd}|ij\rangle\langle ij|V_{dd}|00\rangle}{(E_{00}-E_{ij})^2} = 0.1\,\Delta E^s_{\rm hf}, \quad (3)$$

where the ratio of the tensor to scalar matrix shifts $\Delta E^t_{\rm hf}/\Delta E^s_{\rm hf} \leqslant A_P/A_S = 0.1$ for Rb [8]. This is consistent with the fact that the third-order tensor Stark shifts of alkali-metal atoms are suppressed by a factor of $\simeq$100 compared to the scalar shifts [17]. Note also that the ratio of third-order tensor and scalar polarizabilities of atomic Cs, $\alpha_2^{(3)}/\alpha_0^{(3)} = 0.03$ [17], is four times smaller than the upper bound (3).

To obtain the dispersion energy needed to estimate the tensor matrix shift via Eq. (3), we carried out accurate *ab initio* calculations of the Rb-H_2 interaction potential using the unrestricted coupled cluster method with single, double, and perturbative triple excitations [UCCSD(T)] [18]. A large augmented correlation-consistent polarization valence quadruple-ζ basis set (aug-cc-pVQZ) [19] and the ECP28MDF relativistic effective core potential with the $[13s10p5d3f]$ basis set [20] were used for the H and Rb atoms, respectively. The

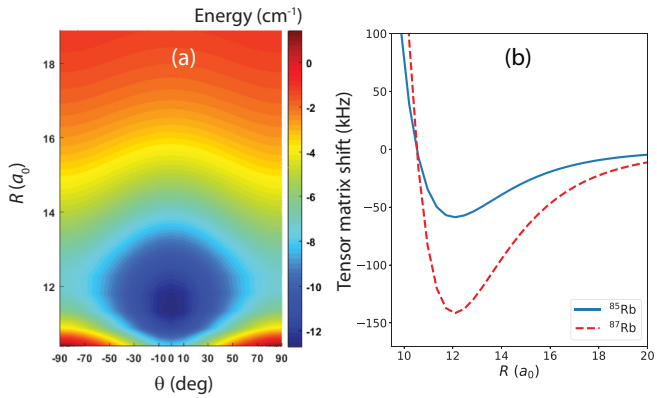

FIG. 4. (a) *Ab initio* PES for Rb-H_2 plotted as a function of the Jacobi coordinates R and θ. (b) Tensor matrix shifts of ^{85}Rb (solid line) and ^{87}Rb (dashed line) interacting with six p-H_2 molecules as a function of the Rb-H_2 distance R.

basis set superposition error for Rb-H_2 interaction energy was corrected using the standard approach [21]. All calculations were carried out with the MOLPRO suite of programs [22]. The potential energy surface (PES) is expressed in the Jacobi coordinates R and θ, where R is the distance between the Rb atom and the H_2 center of mass, and θ is the angle between the atom-molecule vector $\mathbf{R}$ and the H_2 axis. To obtain the effective Rb-H_2 potential $V_0(R)$ used in matrix shift calculations, we averaged 19 PES cuts corresponding to evenly spaced values of $\theta \in [0^\circ, 90^\circ]$ using the hindered rotor model [23]. A contour plot of our *ab initio* PES shown in Fig. 4(a) demonstrates that the Rb-H_2 interaction is weakly anisotropic.

Figure 4(b) shows our calculated upper bounds to the tensor matrix shifts of Rb as a function of the Rb-H_2 distance R, calculated for six p-H_2 molecules. The theoretical bounds are consistent with the measured values shown in Fig. 3, reaching their maxima of 59 kHz for ^{85}Rb and 142 kHz for ^{87}Rb near the minimum of the potential well. The large magnitude of the shift in ^{87}Rb is due to its larger hyperfine constant, which exceeds that of ^{85}Rb by a factor of 3.4. The R dependence of the shifts follows that of the Rb-H_2 interaction energy, reaching a minimum at $R_e \simeq 12.1a_0$ and tending to zero at large R. At short values of R to the left of the potential minimum, the dominant mechanism responsible for the matrix shifts is no longer the dispersion interaction, but rather the Pauli exclusion force arising from the overlap of the electronic wave functions of Rb and H_2 [15]. Thus, our matrix shift estimates at $R \ll 12a_0$ should not be considered even qualitatively accurate. We also note that the calculated tensor matrix shifts scale with m_F (for a given isotope and F) as m_F^2 due to the second-rank tensor nature of the magnetic dipole hyperfine interaction in the excited atomic states [17].

In conclusion, we have established that the spin dephasing of Rb atoms in parahydrogen at densities $\lesssim 10^{18}$ cm^{-3} is dominated by interactions that are electrostatic (or "T-even") in nature. As such, the T_2^* can be significantly increased by replacing traditional Larmor precession states (or traditional single-photon EPR spectroscopy) with superposition states of (or multiphoton transitions between) Zeeman levels that are time reversals of each other.

This will enable greater resolution in EPR spectroscopy, and is of use for improving ensemble magnetometry [24,25] and for fundamental physics experiments with atoms and molecules in matrices [26,27]. We note that for these applications, the superposition states we have explored have two advantages: Their inhomogeneous broadening is reduced and they evolve phases faster than Larmor precession states, limited to a factor of $2F$ for the stretched states. The latter advantage has been explored in recent work with dysprosium atoms [28] and with mechanical oscillators [29], where larger factors can be achieved.

Our results are similar to the "double quantum coherence magnetometry" techniques developed for nitrogen vacancy (NV) centers in diamond [24,25,30,31], but in a different limit. NV centers are typically used in the regime where the electrostatic coupling of the spin to the lattice is $\gg$ its coupling to B_z; here, we work in a limit where the coupling to B_z is $\gg$ the electrostatic coupling to the matrix. The NV-center limit requires the use of a single-crystal sample with magnetic field parallel to the crystal axis [24]; in the current work we employ what we expect is a polycrystalline sample [11,12], and see no dependence of the FID linewidths on the magnetic field direction. We speculate the electrostatic broadening comes from a combination of inhomogeneous trapping sites and inhomogeneous crystal axis orientations.

Our narrowest observed linewidth of 5 kHz corresponds to a T_2^* of 60 μs. We note this ensemble T_2^* is longer than reported values for ensembles of NV centers in diamond [24]. It is also, surprisingly, an order of magnitude longer than reported for alkali-metal atoms in superfluid helium [32]. The only condensed-phase electron spin system with longer reported ensemble T_2^* times is atomic cesium in solid He, which was measured at a significantly lower spin density [33].

We expect even longer T_2^* times can be obtained in parahydrogen by employing stretched-state superpositions and by producing single-crystal samples through different growth parameters or sample annealing [11,12].

This material is based upon work supported by the National Science Foundation under Grants No. PHY-1607072, No. PHY-1607610, and No. CHE-1654547. We gratefully acknowledge assistance in the construction of the experimental apparatus from Wade J. Cline and Carl D. Davidson, Jr. We thank Andrei Derevianko and Amar C. Vutha for valuable conversations and thank Pierre-Nicholas Roy for providing the hindered rotor code.

[1] D. Budker and M. Romalis, Nat. Phys. **3**, 227 (2007).

[2] S. A. Al'Tshuler and B. M. Kozyrev, *Electron Paramagnetic Resonance* (Academic, New York, 1964).

[3] V. Andreev, D. G. Ang, D. DeMille, J. M. Doyle, G. Gabrielse, J. Haefner, N. R. Hutzler, Z. Lasner, C. Meisenhelder, B. R. O'Leary, C. D. Panda, A. D. West,

E. P. West, X. Wu (ACME Collaboration), Nature (London) **562**, 355 (2018).

[4] S. Pustelny, D. F. Jackson Kimball, C. Pankow, M. P. Ledbetter, P. Wlodarczyk, P. Wcislo, M. Pospelov, J. R. Smith, J. Read, W. Gawlik *et al.*, Ann. Phys. **525**, 659 (2013).

[5] J. M. Brown, S. J. Smullin, T. W. Kornack, and M. V. Romalis, Phys. Rev. Lett. **105**, 151604 (2010).

[6] S. Upadhyay, A. N. Kanagin, C. Hartzell, T. Christy, W. P. Arnott, T. Momose, D. Patterson, and J. D. Weinstein, Phys. Rev. Lett. **117**, 175301 (2016).

[7] A. N. Kanagin, S. K. Regmi, P. Pathak, and J. D. Weinstein, Phys. Rev. A **88**, 063404 (2013).

[8] E. Arimondo, M. Inguscio, and P. Violino, Rev. Mod. Phys. **49**, 31 (1977).

[9] W. Weltner, *Magnetic Atoms and Molecules* (Courier Corporation, North Chelmsford, MA, 1989).

[10] See Supplemental Material at http://link.aps.org/supplemental/10.1103/PhysRevB.100.024106 for a detailed comparison of our measurements of T_2^* by FID and depolarization spectroscopy.

[11] S. Tam, M. E. Fajardo, H. Katsuki, H. Hoshina, T. Wakabayashi, and T. Momose, J. Chem. Phys. **111**, 4191 (1999).

[12] P. L. Raston, S. C. Kettwich, and D. T. Anderson, J. Chem. Phys. **139**, 134304 (2013).

[13] D. A. Steck, Rubidium 85 D line data, https://steck.us/alkalidata/ (2013) .

[14] V. A. Dzuba, V. V. Flambaum, K. Beloy, and A. Derevianko, Phys. Rev. A **82**, 062513 (2010).

[15] F. J. Adrian, J. Chem. Phys. **32**, 972 (1960).

[16] P. Moroshkin, A. Hofer, and A. Weis, Phys. Rep. **469**, 1 (2008).

[17] S. Ulzega, A. Hofer, P. Moroshkin, and A. Weis, Europhys. Lett. **76**, 1074 (2006).

[18] M. J. O. Deegan and P. J. Knowles, Chem. Phys. Lett. **227**, 321 (1994).

[19] T. H. Dunning, J. Chem. Phys. **90**, 1007 (1989).

[20] I. S. Lim, P. Schwerdtfeger, B. Metz, and H. Stoll, J. Chem. Phys. **122**, 104103 (2005).

[21] S. F. Boys and F. Bernardi, Mol. Phys. **19**, 553 (1970).

[22] H.-J. Werner, P. J. Knowles, G. Knizia, F. R. Manby, and M. Schütz, Wiley Interdiscip. Rev.: Comput. Mol. Sci. **2**, 242 (2011).

[23] H. Li, P.-N. Roy, and R. J. Le Roy, J. Chem. Phys. **133**, 104305 (2010).

[24] E. Bauch, C. A. Hart, J. M. Schloss, M. J. Turner, J. F. Barry, P. Kehayias, S. Singh, and R. L. Walsworth, Phys. Rev. X **8**, 031025 (2018).

[25] H. J. Mamin, M. H. Sherwood, M. Kim, C. T. Rettner, K. Ohno, D. D. Awschalom, and D. Rugar, Phys. Rev. Lett. **113**, 030803 (2014).

[26] A. Weis, S. Kanorsky, S. Lang, and T. Hänsch, in *Atomic Physics Methods in Modern Research* (Springer, Berlin, 1997), pp. 57–75.

[27] A. Vutha, M. Horbatsch, and E. Hessels, Atoms **6**, 3 (2018).

[28] T. Chalopin, C. Bouazza, A. Evrard, V. Makhalov, D. Dreon, J. Dalibard, L. A. Sidorenkov, and S. Nascimbene, Nat. Commun. **9**, 4955 (2018).

[29] K. C. McCormick, J. Keller, S. C. Burd, D. J. Wineland, A. C. Wilson, and D. Leibfried, arXiv:1807.11934.

[30] P. Huang, X. Kong, N. Zhao, F. Shi, P. Wang, X. Rong, R.-B. Liu, and J. Du, Nat. Commun. **2**, 570 (2011).

[31] K. Fang, V. M. Acosta, C. Santori, Z. Huang, K. M. Itoh, H. Watanabe, S. Shikata, and R. G. Beausoleil, Phys. Rev. Lett. **110**, 130802 (2013).

[32] M. Koch, G. Auböck, C. Callegari, and W. E. Ernst, Phys. Rev. Lett. **103**, 035302 (2009).

[33] S. I. Kanorsky, S. Lang, S. Lücke, S. B. Ross, T. W. Hänsch, and A. Weis, Phys. Rev. A **54**, R1010 (1996).